16 May 1997

ELSEVIER

Chemical Physics Letters 270 (1997) 196–205

CHEMICAL PHYSICS LETTERS

Charge flow and solvent dynamics in the photodissociation of cluster ions: a nonadiabatic molecular dynamics study of $I_2^- \cdot Ar_n$

J. Faeder, N. Delaney, P.E. Maslen [1], R. Parson

JILA and Department of Chemistry and Biochemistry, University of Colorado and National Institute of Standards and Technology, Boulder, CO 80309-0440, USA

Received 30 January 1997; in final form 3 March 1997

Abstract

Experimental studies of photodissociation in $I_2^- \cdot Ar_n$ clusters have shown a rapid onset of caging for $n > 10$ and bimodal photofragment distributions in both dissociation and recombination channels. We simulate and interpret these results using a Hamiltonian that accounts for the strong perturbation of the solute electronic structure by the solvent. The high-mass products in the recombination channel are identified with excited state recombination. The two classes of dissociation products are identified with ejection of either a neutral I atom or an I^- ion from the cluster, with the latter mechanism driven by the negative polarizability of the excited electronic state. © 1997 Elsevier Science B.V.

1. Introduction

In a recent experiment, Lineberger and coworkers [1–3] have studied the photodissociation of I_2^- molecular anions embedded in size-selected clusters containing 1 to 27 argon atoms. As had previously been found for I_2^- clustered with CO_2 [4], the presence of the solvent argon atoms around the I_2^- solute can force the I atoms to recombine after dissociation, a process known as caging. The relative abundance of recombined products increases smoothly but rapidly with the number n of argon atoms in the precursor cluster, from zero for $n \leq 10$ to 100% for $n \geq 16$.

When the recombined products are analyzed according to their mass, they fall into two classes. In the first, all or nearly all of the argon atoms have been lost, indicating that I_2^- has relaxed to the neighborhood of its vibrational ground state with the excess energy being removed by evaporation of argon atoms. In the second, referred to as "metastable," a much larger number of argon atoms remains bound to the solute. Vorsa et al. [1] infer that in these products ground-state I_2^- has not been formed, and suggest two possibilities for the metastable species: a solvent separated pair in which I and I^- are separated by one or more argon atoms, or a trapped excited state in which the I atoms have recombined into the weakly bound $^2\Pi_{g,3/2}$ state (see Fig. 1). Provided that evaporation is able to cool such species to low vibrational states in the excited electronic state, they are expected to be relatively stable since collision-induced electronic transitions will be highly improbable when the molecule is near its equilibrium geometry. Further evidence for this interpretation is found in recent femtosecond time-resolved pho-

[1] Current address: Department of Chemistry, University of California, Berkeley, CA 94720, USA.

PII S0009-2614(97)00335-7

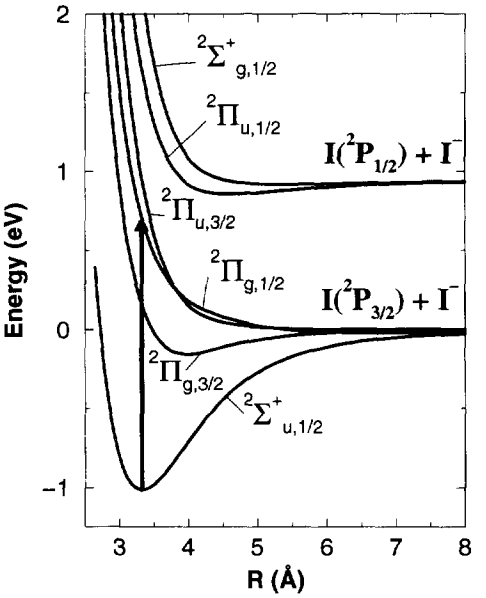

Fig. 1. Scaled ab initio gas phase potential curves for I_2^-. The arrow shows the 790 nm photoexcitation to the $^2\Pi_{g,1/2}$ state modeled in the current simulations.

todetachment experiments by Neumark and coworkers [5]. The transient photodetachment spectrum of the photodissociation products displays a shift that can be attributed to the formation of I_2^- in an excited electronic state.

In the smaller precursor clusters, where caging is incomplete, Vorsa et al.[1] find a bimodal distribution in the *dissociated* products as well. At $n = 13$, for example, the I^- based products fall into two distinct groups, one having 0–3 argon atoms and the other having 5–7 argon atoms. The average number of remaining argon atoms in the second group scales linearly with the precursor cluster size, but the average number in the first group is independent of cluster size.

In this letter, we use nonadiabatic MD simulations to elucidate the mechanisms that give rise to the various product channels observed in the experiment. Photodissociation of molecular cluster ions presents a major challenge for such simulations, since the polarized solvent strongly perturbs the electronic structure of the solute. We treat these perturbations by means of an effective Hamiltonian, constructed by evaluating the solvent–solute interaction in the representation defined by ab initio electronic states of the isolated solute. At each step of the simulation this Hamiltonian is diagonalized, providing the the energies, forces and nonadiabatic transition probabilities required to propagate the trajectories. The results of our simulation reproduce the observed trends in the experimental dissociation probabilities and branching ratios. For the recombined photofragments, we find no evidence for solvent-separated pairs but we do find significant recombination into the excited state. For dissociated fragments, we find that the low-mass product channel arises from ejection of an I^- ion from the cluster. This peculiar dissociation mechanism is driven by "anomalous charge switching" [6] in the $^2\Pi_{g,1/2}$ excited state. The parallel polarizability of I_2^- in this state is negative, so that charge flows towards the less solvated atom.

2. Methods

We treat the solute as a diatomic molecule whose electronic states are perturbed by the interaction with the solvent, assuming that there is no charge transfer to the solvent. Since the solute electronic states become nearly degenerate as the molecule dissociates, they can be strongly mixed by even a relatively weak perturbation. We account for this mixing by constructing a Hamiltonian using as a basis the lowest six electronic states of the bare I_2^- ion, obtained from a recent *ab initio* calculation [7]. Within this basis we compute the matrix elements of the solute–solvent interaction, which couple the states of the isolated molecule. The interaction between the charge distribution of the I_2^- ion and the induced moments on the polarizable argon atoms is responsible for most of the coupling in this system. By diagonalizing this Hamiltonian and taking its derivatives, we obtain the energies, forces and nonadiabatic couplings required for a full treatment of the dissociation dynamics on the multiple electronic potential energy surfaces. The eigenstates also allow us to compute properties of the solute, such as the charge distribution and the transition moments, which are vital for understanding the dynamics and for making comparisons between the model and experiment.

2.1. Model Hamiltonian

We write the Hamiltonian of the solute–solvent system

$$\hat{H} = \hat{h}^C + \sum_A \hat{h}^A + \hat{H}^{\text{ind}} + \hat{H}^{\text{sr}}, \quad (1)$$

where $\hat{h}^C$ and the $\hat{h}^A$ are the Hamiltonians of the solute and solvent respectively, $\hat{H}^{\text{ind}}$ describes the induction and low frequency dispersion interactions between the charge distribution of the solute and the polarizable solvent, and $\hat{H}^{\text{sr}}$ represents the short-range solute–solvent and solvent–solvent interactions arising from dispersion and repulsion. Since the solvent is confined to its ground electronic state, the $\hat{h}^A$ terms are constants and are left out of the calculations.

The lowest six electronic states of the isolated solute form the basis for evaluating $\hat{H}$. $\hat{h}^C$ is clearly diagonal in this representation, and the I_2^- potential curves which define it are shown in Fig. 1. Although the two electronic states that dissociate to give spin-orbit excited iodine do not participate directly in the photodissociation dynamics investigated here, their presence in the basis is important for an accurate description of the $^2\Pi_{g,1/2}$ wavefunction, which undergoes a fundamental shift in character as the molecule dissociates [7]. The depth of the ground $^2\Sigma^+_{u,1/2}$ state well has been scaled from the ab initio value of 0.905 eV to bring it into agreement with the most recent experimental value of 1.01 eV [8]. The equilibrium bond length R_e of the scaled ground state is 3.32 Å. The excited states have also been scaled by holding the energy difference with the ground state fixed at the *ab initio* value. R_e and D_e of the scaled $^2\Pi_{g,3/2}$ are 3.96 Å and 158 meV. Each of the states shown has a two-fold spin degeneracy, bringing the total number of basis states to 12. While interactions with the solvent do not lift this degeneracy, the full Hamiltonian does not factorize in a way that makes it possible to reduce its dimension [6].

The properties of the solute electronic wave functions are represented in the form of distributed multipole operators [9,10]. Moments up through the quadrupole are included on each of four expansion sites, one on each iodine atom and two along the bond (these bond sites are removed as the molecule dissociates). The diagonal elements of the distributed multipole operators provide an accurate representation of the charge distribution in each electronic state. In a polar solvent, for example, diagonal matrix elements of the solute–solvent interaction Hamiltonian would arise from the charge distribution of each electronic basis state interacting with the charge distribution of the solvent. The off-diagonal distributed multipole operators represent *transition charge densities* and give rise to coupling between the electronic basis states in the presence of an electric field, thus allowing the solute molecule to polarize in response to the solvent. Because all of the low-lying states of I_2^- are included in the model, the off-diagonal distributed multipoles should provide a reasonably accurate representation of the solute polarizability.

The lowest order interactions between I_2^- and the argon cluster arise from electronic polarization of the solvent. This is a collective, many-body effect involving distortion of the charge clouds on both solute and solvent molecules. We assume that the time scale for polarization fluctuations in the solvent is much shorter than that for charge flow in the solute [11–13]. This limit should be valid here since the electronic excitation energy of argon is much larger than the energy gaps between the first few excited states of I_2^-. Following Stone's compact notation for the multipole moments and interaction tensors [10,14], the induction Hamiltonian may be written as [15]

$$\hat{H}^{\text{ind}} = -\tfrac{1}{2}\hat{\mu}^A(\alpha^{AA})^{-1}[1 + \alpha^{AA}T^{AA}]^{-1}\hat{\mu}^A, \quad (2)$$

$$\hat{\mu}^A \equiv -\alpha^{AA}T^{AC}\hat{q}^C, \quad (3)$$

where $\hat{q}^C$ is the solute distributed multipole operator, α is the solvent polarizability tensor, T^{AA} is the interaction tensor between solvent atoms, and T^{AC} is the interaction tensor between solvent atoms and the solute distributed multipole sites. $\hat{\mu}^A$ represents the multipoles induced on solvent molecules by the distributed multipole moments $\hat{q}^C$ on the solute. Since we include only the dipole polarizability of argon (11.07 au [16]), the $\hat{\mu}^A$ are simply the first order induced dipole moments on the solvent atoms. The inverse term in brackets in Eq. (2) implicitly takes into account the mutual interaction of the polarized solvent molecules. Constructing it is equivalent to solving the familiar equilibrium linear response equation [10] for the induced dipoles, and computing the quantity $(1 + \alpha^{AA}T^{AA})^{-1}\hat{\mu}^A$ is equivalent to iterating the induced solvent dipoles to self-consistency. If the induced dipole operators were replaced by classical variables, Eq. (2) would be simply the classical induction energy of the solute electrons in the field of the polarized solvent.

The short-range interactions are described by pairwise-additive potentials. The Ar–Ar interactions are modeled by an isotropic Lennard-Jones potential with R_e and D_e fit to match experimental values [17]. Fitting the Ar–I potential is complicated by the fact that this interaction depends on the orientation of the empty p orbital on the iodine atom. This anisotropy is physically important because it enables the argon solvent atoms to reorient the p orbital hole on the I atoms, and thus to change the molecular Ω quantum number. Without inclusion of this anisotropy, no excited state recombination is observed in the model. The anisotropy is modeled by adding a $1/R^6$ short-range interaction term having the same angular and state dependence as an ion-quadrupole interaction; this is equivalent to expanding the angular dependence of the potential in Legendre polynomials and retaining the first nonvanishing anisotropic term, proportional to $P_2(\cos\theta)$. This term, together with an isotropic Lennard-Jones potential, enables us to obtain a good fit to the experimental potential curves for both the I–Ar and the I^-–Ar interactions, determined from photodetachment spectra [18].

The model Hamiltonian enables us to compute the six-state multidimensional potential surface of arbitrary-sized $I_2^-(Ar)_n$ clusters. In order to carry out molecular dynamics and surface hopping, we must be able to compute derivatives of the Hamiltonian matrix elements with respect to all of the nuclear coordinates. We refer the reader to Ref. [6] for the details of how this is done, but mention here that computation of the derivatives is greatly simplified by the use of Stone's notation and formulae for the electrostatic interaction tensors and their derivatives [10,14].

2.2. *Structure, dynamics and surface hopping*

Molecular dynamics trajectories are computed on the model potential surfaces using the velocity version of the Verlet algorithm [19]. The ensembles used to study the photoexcitation dynamics were composed of 41 configurations obtained following an initial equilibration of 10–20 ps by sampling a 400 ps trajectory at an interval of 10 ps. A timestep of 10 fs was found to give adequate energy conservation during the equilibration period. The photoexcitation process was simulated by placing the the solute in the $^2\Pi_{g,1/2}$ state after adjusting the I_2^- bondlength so that the initial energy gap between the ground and excited states matched the 790 nm photon energy. The maximum bondlength adjustment required was about 0.04 Å, so this procedure had little effect on the initial configurations except to scale the total kinetic energy release on the excited state to approximately the experimental value. Ensembles were prepared at two temperatures, roughly 40 and 50 K, for the cluster range $n = 6$, 8–17, 20. These temperatures, chosen to match the 40 K estimate of the cluster temperature in the experiments [1], roughly straddle the solid–liquid phase transition region [20]. The underlying cluster structure was also investigated by performing conjugate gradient optimizations [21] on the equilibrated ensembles.

To simulate the nonadiabatic dynamics during the photodissociation, we follow the recent surface-hopping method of Tully [22]. In this method the quantum state amplitudes are integrated along a trajectory using the time-dependent Schrödinger equation

$$i\hbar\dot{c}_i = \sum_j c_j(E_i\delta_{ij} - i\hbar\dot{\boldsymbol{R}}(t)\cdot\boldsymbol{d}_{ij}), \tag{4}$$

where c_i is the quantum amplitude for state i, E_i is the energy of adiabatic state i, $\dot{\boldsymbol{R}}(t)$ is a vector containing all of the nuclear velocities, and $\boldsymbol{d}_{ij}$ is the nonadiabatic coupling vector between states i and j. At each time step the probability of hopping to another state is computed, and the occurrence of a hop is determined probabilistically using Tully's "least switches" algorithm [22]. This algorithm minimizes the total number of hops along a given trajectory while ensuring that the fraction of the total ensemble in a given quantum state will approach the probabilities given by the integration of Eq. (4).

When a hop occurs, the velocities are scaled to preserve energy conservation, and the hop is rejected if this scaling cannot be performed. Ref. [23] describes an additional "velocity reversal" procedure, in which the velocities in the direction of the nonadiabatic coupling are reversed following a rejected hop. This procedure was not used in simulation results presented here, and we have found that including this scaling does not affect the final product distributions.

Simply integrating Eq. (4) along an entire trajectory has been shown to give incorrect transition probabilities arising from spurious coherence effects [22,24]. Following the analysis suggested by Schwartz et al., we have estimated the quantum de-

coherence times for this system to be 100–200 fs in the coupling regions. The current results have been obtained from trajectories in which the quantum amplitudes are reset at an interval of 100 fs. We have found that increasing this interval and/or resetting the amplitudes only in regions of weak coupling have no significant effect on the product distributions.

Following photoexcitation, trajectories were run with a fixed classical timestep of 2 fs, while the quantum amplitudes were integrated using an adaptive Runge-Kutta method [21] with a much smaller time step. The quantities $E_i(t)$ and $\dot{\boldsymbol{R}}(t) \cdot \boldsymbol{d}(t)_{ij}$ were computed at the intermediate steps of the adaptive integration by the interpolation and extrapolation methods described in Ref. [23]. In regions of strong nonadiabatic coupling the classical timestep was also made shorter to ensure accurate calculation of the transition amplitudes. The trajectories were continued until the nuclear configurations met one of two product criteria: dissociative products, where the I–I distance surpassed the cutoff distance of 30 Å, or recombined products, where I_2^- had undergone more than 10 vibrational oscillations in a particular potential well. The time to product formation ranged from 5 to 50 ps. The product criteria were carefully tested and we believe the branching ratios for the model have been accurately determined. The product mass distributions are also reasonably accurate, but should be shifted to lower solvent mass due to the relatively short trajectory lengths and the long times required to evaporate the final argon atoms.

3. Results

Fig. 2 shows the binding energy of each argon atom added to the cluster for the lowest energy structures of $I_2^- \cdot Ar_n$, along with the particularly stable structures obtained for n = 6, 13 and 20. The optimized structures show that the argon shell is built up by formation of six-membered rings. The first ring forms around the I_2^- waist, the second around one end of the solute. A single argon atom caps the end, completing the half-shell configuration shown in the middle of Fig. 2. The filling of the third ring with cap completes the solvation shell around I_2^- at n = 20. Although two more atoms may crowd the cap positions in n = 21 and 22, these structures are somewhat strained. Each

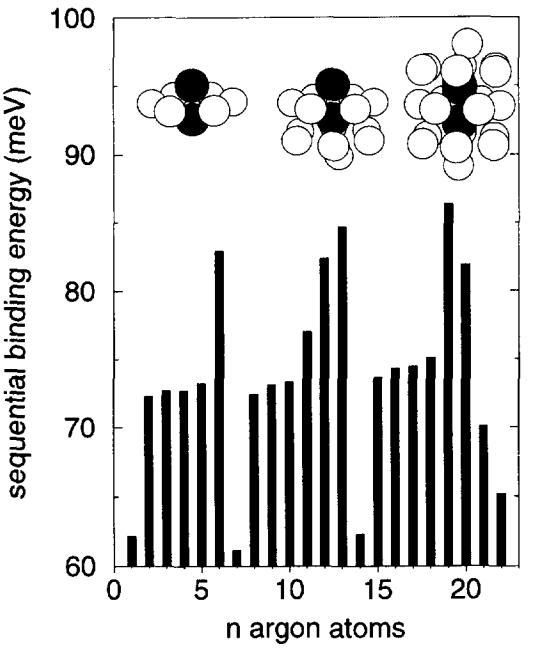

Fig. 2. Sequential binding energies of argon to I_2^- obtained from the lowest energy structures. The energy for adding the nth argon atom is plotted, and the structures of "magic number" clusters for n = 6, 13 and 20 are shown.

completion of a ring or filling of a cap site produces a structure of greater relative stability. The most stable structures at n = 6, 13 and 20 correspond exactly to the noted peaks in the exerimental mass spectrum [1], suggesting that the model potential captures the essential structural features of these clusters.

The dissociative trajectories produce two distinct classes of $I^- \cdot Ar_m$ products for the precursor cluster range $11 \leq n \leq 14$. The low-mass products, $m \leq 2$, result from direct ejection of I^- from the cluster. This process is depicted in Fig. 3a. The initial configuration, with solvent atoms bound primarily to one end of the cluster, is typical of clusters in this size range and illustrates what we call "asymmetric solvation." The I_2^- dissociates rapidly passing 10 Å separation in the first picosecond of the trajectory, during which the charge localizes on the less solvated I atom. The initially solvated atom is arrested quickly by the solvent. I^- is slowed by its attraction to the solvent but escapes dragging a single argon atom. During the I^- escape there is no opportunity for charge transfer because the energies of the states with different charge character remain well-separated. The formation of the low-mass

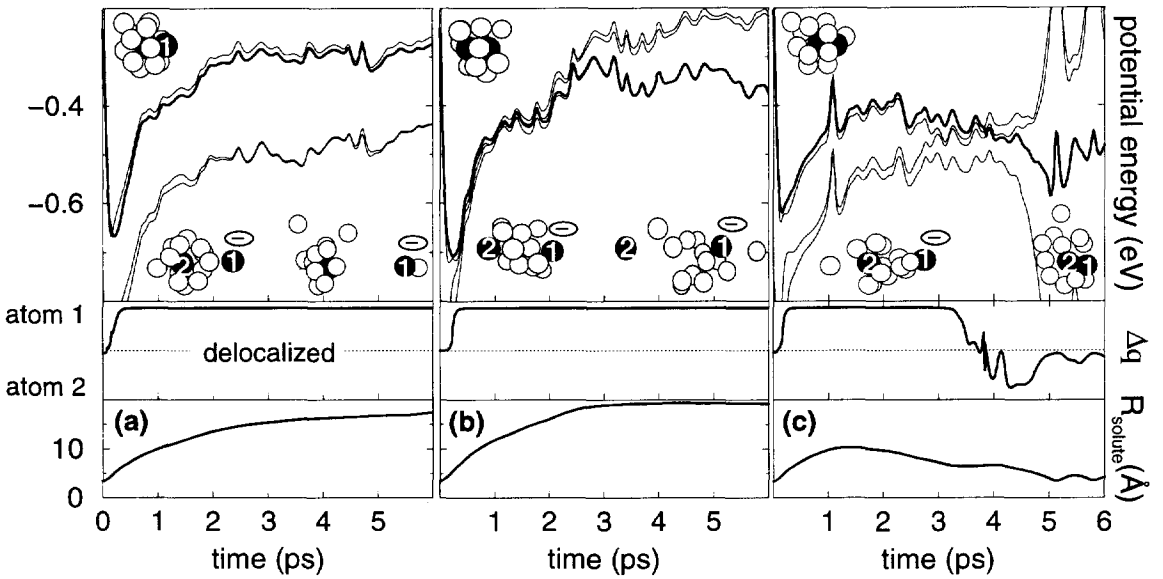

Fig. 3. Photodissociation of $I_2^-\cdot Ar_{13}$. The adiabatic energies, the location of the charge (Δq), and the I–I distance are plotted as a function of time. The heavier line in the top panel shows the energy of the currently occupied state. Snapshots of the configurations showing the localization of the charge are shown at t = 0, 1 and 5 ps. (a) shows a dissociative trajectory which forms $I^-\cdot Ar_1$ and $I\cdot Ar_9$ as a direct result of the anomalous charge switching. (b) shows a dissociative trajectory which forms $I^-\cdot Ar_7$ and I following solvent transfer from atom 2 to atom 1 during the first few ps. (c) shows a trajectory which recombines in the excited electronic state ultimately forming $I_2^-\cdot Ar_5$. Near 4 ps a charge transfer takes place returning the I_2^- to a normal charge switching state where it recombines and the charge delocalizes.

I^- product is also accompanied by the production of a large neutral cluster, $I\cdot Ar_9$.

Fig. 3b shows a trajectory which dissociates to form highly solvated I^-. The initial solvent configuration is more symmetric around I_2^- than in Fig. 3a, and the solvent atoms are in a better position to catch the escaping I^-. By 1 ps solvation of the two I atoms is roughly equal, and further solvation of I^- produces electronic relaxation to a normal charge switching state by about 2 ps. Charge transfer to atom 2 is precluded because of the large I–I separation (>10Å) at these times. The rapid transfer of the solvent facilitates the escape of the neutral I atom, which is notably faster than the escape of I^- in Fig. 3a. The neutral escapes faster because of its weaker attraction to the remaining cluster, leaving behind $I^-\cdot Ar_7$.

The distinct dissociative channels produce a bimodal distribution of $I^-\cdot Ar_m$ products similar to that observed in the experiments. Fig. 4 shows the product distribution for the $I_2^-\cdot Ar_{12}$ precursor. The two modes are present for all precursors in the range n = 11–14 but merge for $n \leq 10$. As in the experiment, the

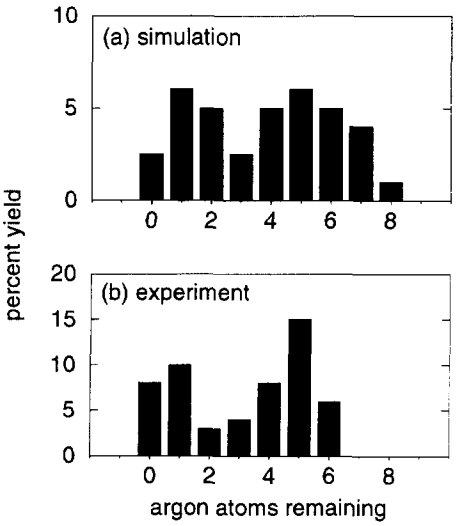

Fig. 4. I^-Ar_m product distributions from the $I_2^-Ar_{12}$ precursor. For this cluster size the simulation gives 39% dissociation compared to 54% in the experiment. The simulated distribution is expected to shift to slightly lower mass as the trajectories are extended in time.

center of the high-mass distribution increases with cluster size, while the low-mass distribution remains centered around $m = 0$ or 1.

Fig. 3c shows a trajectory which recombines in the excited $^2\Pi_{g,3/2}$ state. The initial solvent asymmetry is intermediate between the trajectories shown in Fig. 3a and 3b. The solvent arrests the escape of I^- by about 2 ps, but the solvent interactions are not strong enough to induce electronic relaxation until the solute internuclear separation has returned to about 6 Å. Electronic relaxation occurs via transfer of the charge to atom 2 at around 4 ps. During the subsequent recombination in the excited electronic state, the charge again becomes delocalized. Trajectories which recombine in the ground electronic state are qualitatively similar to the one shown in Fig. 3c.

Roughly half of the trajectories which produce I_2^--based products recombine in the ground electronic state, and the other half recombine in the excited $^2\Pi_{g,3/2}$ state. We do not observe any I_2^--based products where solvent atoms separate the two iodine atoms. Recombination on the $^2\Pi_{g,3/2}$ state appears to produce excited-state I_2^- products with very high efficiency, despite the shallow well depth of this state. Very few trajectories that pass R_e of I_2^- during recombination in the excited state subsequently dissociate to form other products. No dissociation is observed when recombination proceeds past R_e in the ground electronic state.

The branching between recombination in the ground and excited states produces a bimodal product distribution of I_2^--based photofragments. This separation in the product masses arises from the approximately 850 meV difference in the binding energy of the two electronic states on which recombination occurs. Recombination in the excited state releases far less energy and therefore evaporates significantly fewer argon atoms. The trajectories have not all been run for long enough to resolve accurate photofragment distributions for the recombined products, but the large separation in the product channels shows up even at short times. Fig. 5 shows the overall branching ratios for photofragmentation from ensembles with an initial temperature of 50 K and demonstrates the generally good agreement between the model and experimental results. The error bars shown in Fig. 5 represent the statistical sampling error which arises from the relatively small size

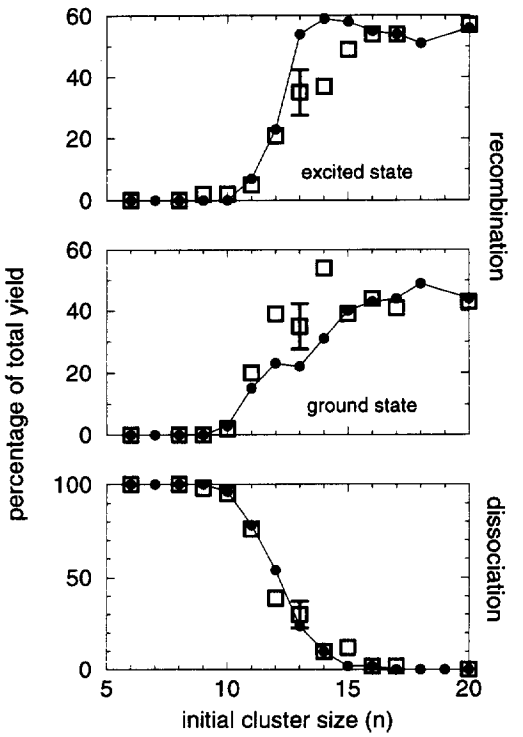

Fig. 5. Branching ratios for the products of $I_2^-Ar_n$ photdissociation at 790 nm. The filled circles are the experimental data and the squares show the simulation results. One σ error bars based on the statistical sampling are shown for $n = 13$. These ranges are representative of the errors at other sizes since all of the ensembles contained 41 trajectories.

of the ensembles. We have generated much larger ensembles for selected cluster sizes and verified that the branching ratios are converged to within the estimated error limits. The simulations reproduce particularly well the rapid closing of the dissociative channel between $n = 10$ and $n = 16$. However, the dissociative branching depends strongly on the temperature of the initial ensemble, so it is premature to make much of the quantitative agreement. This surprising temperature dependence might be associated with what appears to be a solid–liquid phase transition in the 35–50 K range [20]. The simulation results also agree well with the experimental finding of roughly equal amounts of low- and high-mass I_2^--based products. The branching between these two products, which we attribute to ground and excited state recombination respectively, deviates somewhat from the experimental results at intermediate cluster sizes but approaches the

same limit in the larger clusters.

4. Discussion

The ejection of I^- during dissociation is the most surprising finding of this study, and the mechanism by which this process occurs provides the key to understanding fundamental aspects of the photodissociation dynamics. The explanation for I^- ejection lies in the electronic properties of the $^2\Pi_{g,1/2}$ state on which dissociation takes place: the component of the polarizability parallel to the molecular axis is negative, so that *charge tends to flow towards the less favorably solvated atom* [6,25]. This behavior, which we have called "anomalous charge switching," may be understood by considering the eigenfunctions of a particle in a slightly asymmetric double well, or the bonding and antibonding states of a heteronuclear diatomic molecule. In each example, the ground state wave function localizes on the lower-energy well or atom, so by orthogonality the excited state wave function must be polarized in the opposite direction.

Anomalous charge switching arises in our problem because the $^2\Pi_{g,1/2}$ state dissociates to $I{\cdot}Ar_m + I^-$ instead of the normal charge-switching asymptote, $I^-{\cdot}Ar_m + I^*$. The asymptotic behavior is determined by spin-orbit coupling, so if a lighter halide such as chlorine were substituted for iodine, the asymptote would become $Cl^-{\cdot}Ar_m + Cl^*$, and the charge would switch normally.

Anomalous charge switching is evident in the trajectories depicted in Fig. 3. In Fig. 3(a) I^- is produced when the solute remains in the anomalously switching state throughout the trajectory. Charge localization on the less solvated I atom in Fig. 3b leads to solvent transfer at about 2 ps, allowing the escape of the neutral I atom. In Fig. 3c the charge resides on the less solvated atom until the solvent induces a charge-transfer near 4 ps which returns the solute to a normal charge switching state where it recombines.

The first two trajectories demonstrate that low-mass I^- products can arise from the same low temperature precursors as the high-mass products. This finding contrasts with the proposal of Vorsa et al.[1] that the low-mass products arise from high-energy isomers in which the I_2^- is bound to the surface of an argon cluster. We have found by simulating the proposed high-energy isomers that the ion dissolves rapidly into the argon clusters on the timescale of about 50 ps, and thus such species are unlikely to survive the 50–100 μs trip from cluster formation to photolysis. Vorsa et al. based their proposal on the supposition that the low- and high-mass product channels are separated in energy by about 300 meV and thus are unlikely to arise from precursors similar in energy. The trajectory in Fig. 3a illustrates, however, the unexpected result that anomalous charge switching leads to the formation of a highly solvated neutral product which lowers the overall energy of the low-mass channel.

Anomalous charge switching also plays a role in the rapid onset of caging and the closing of the dissociative channels for $10 \leq n \leq 16$. The asymmetric solvation of the initial clusters in this range combined with the flow of charge onto the less solvated atom results in an ion rather than a neutral atom trying to escape from the cluster. The ion–induced-dipole forces thus tend to pull the clusters back together where electronic relaxation and recombination into the lower state potential wells are likely to occur. A simple energetic argument may explain the onset of recombination around $n = 9$ or 10. In both simulation and experiment, the binding energy of a single Ar atom is estimated to be about 70 meV; combining this with the photon energy of 790 nm, the I_2^- binding energy of 1.01 eV, and a nominal initial cluster temperature of 40 K, we estimate that at least eight argon atoms must be evaporated in order to reduce the energy of I_2^- below the dissociation limit. The closing of the dissociation channel well before the completion of the first solvent shell may result from the fact that for $n > 13$ additional argon atoms are forced to solvate the other iodine, creating a more symmetric solvent distribution and placing the argon atoms in a better position to catch the escaping ion.

One final issue is what determines the state in which the recombination takes place. Both experiment and simulation show approximately equal branching between the two recombination channels, with a slight propensity for the excited state. Since at long bond lengths the two states differ only in the alignment of the empty p orbital on the iodine atom with respect to the molecular axis, this result suggests that the initial alignment of this orbital has been mostly lost by the time the atoms recombine. A small number of I–Ar collisions suffices to reorient the p orbital hole quite efficiently. This result is not surprising since depo-

larization cross sections in the $^2P_{3/2}$ states of heavy atoms are known to be very large [26–28]. The slight propensity for the excited state may result from the simple fact that it is initially closer in energy to the photoexcited state and thus nonadiabatic transitions will more likely.

5. Conclusions

We have used nonadiabatic molecular dynamics simulations to interpret the results of the cluster photofragmentation experiments of Lineberger and coworkers. We find that the two major classes of dissociated products correspond to ejection either of neutral I atoms or of charged I^- ions from the precursor cluster, the latter process being driven by the anomalous charge flow in the excited electronic state. The two major classes of I_2^--based products correspond to recombination into either the ground state or the excited $^2\Pi_{3/2}$ state. This latter conclusion is in accord with those reached by Neumark and coworkers [8] on the basis of time-resolved photodetachment spectra of the photoproducts. The approximately equal branching between ground and excited state recombination suggests that the during the photodissociation/recombination process the orientation of the electron cloud on the I atom is largely randomized by collision with the Ar atoms.

While this research was being prepared for publication, we received a preprint in which Batista and Coker [29] simulate the same system with nonadiabatic molecular dynamics applied to a semiempirical diatomics-in-molecules Hamiltonian. While this Hamiltonian is constructed differently from ours, it appears to contain the same essential physics. There are some differences in detail between their results and ours but the overall trends are in agreement; they also conclude that the high-mass recombined products arise from excited state recombination. The fact that such similar results are obtained from these two substantially different models suggest that both capture the essential features of the problem.

A major finding of this study is that anomalous charge switching in the excited state leads to ejection of a negative ion from the cluster. This mechanism would appear to be peculiar to small clusters, since in large clusters or in the condensed phase an electronic transition to a normal charge-switching state will occur before the ion can escape. However, anomalous charge switching itself may be important for large systems as well as small, particularly for processes that are determined by short time dynamics. We intend to pursue these issues in future publications.

Acknowledgements

We would like to thank Carl Lineberger, Sreela Nandi, John Papanikolas, Vasil Vorsa and Alex Zozulya for their contributions to this project. We are grateful to David Coker for sending us a preprint of Ref. [29], and to Dan Neumark and his group for informing us of their recent time-resolved photodetachment results. We would also like to thank the refereee for several helpful suggestions. This work was supported by Grants Nos. CHE-9217693 and PHY-9012244 from the National Science Foundation.

References

[1] V. Vorsa, P. J. Campagnola, S. Nandi, M. Larsson and W. C. Lineberger, J. Chem. Phys. 105 (1996) 2298.
[2] V. Vorsa, S. Nandi, P.J. Campagnola, M. Larsson and W.C. Lineberger, J. Chem. Phys. 106 (1997) 1402.
[3] V. Vorsa, PhD thesis, University of Colorado (1996).
[4] J.M. Papanikolas, J.R. Gord, N.E. Levinger, D. Ray, V. Vorsa and W.C. Lineberger, J. Phys. Chem. 95 (1991) 8028.
[5] D.M. Neumark, private communication.
[6] P.E. Maslen, J.M. Papanikolas, J. Faeder, R. Parson and S.V. ONeil, J. Chem. Phys. 101 (1994) 5731.
[7] P.E. Maslen, J. Faeder and R. Parson, Chem. Phys. Lett. 263 (1996) 63.
[8] B.J. Greenblatt, M.T. Zanni and D.M. Neumark, Science, submitted.
[9] A.J. Stone, Chem. Phys. Lett. 83 (1981) 233.
[10] A.J. Stone, The Theory of Intermolecular Forces, (Oxford, New York, 1996).
[11] J.N. Gehlen, D. Chandler, H.J. Kim and J.T. Hynes, J. Phys. Chem. 96 (1992) 1748.
[12] R.A. Marcus, J. Phys. Chem. 96 (1992) 1753.
[13] H.J. Kim and J.T. Hynes, J. Chem. Phys. 96 (1992) 5088.
[14] S.L. Price, A.J. Stone and M. Alderton, Mol. Phys. 52 (1984) 987.
[15] P.E. Maslen, J. Faeder and R. Parson, unpublished work.
[16] D. R. Lide, ed., 73rd Ed. CRC Handbook of Chemistry and Physics (Chemical Rubber, Boca Raton, 1993).
[17] K.T. Tang and J.P. Toennies, J. Chem. Phys. 80 (1984) 3726.
[18] Y. Zhao, I. Yourshaw, G. Reiser, C.C. Arnold and D.M. Neumark, J. Chem. Phys. 101 (1994) 6538.

[19] H.C. Andersen, J. Comput. Phys. 52 (1982) 24.
[20] N. Delaney, J. Faeder and R. Parson, To be published, 1997.
[21] W.H. Press, S.A. Teukolsky, W.T. Vetterling and B.P. Flannery, Numerical Recipes in C: The Art of Scientific Computing, 2nd Ed. (Cambridge University Press, New York, 1992).
[22] J.C. Tully, J. Chem. Phys. 93 (1990) 1061.
[23] S. Hammes-Schiffer and J.C. Tully, J. Chem. Phys. 101 (1994) 4657.
[24] B.J. Schwartz, E.R. Bittner, O.V. Prezhdo and P.J. Rossky, J. Chem. Phys. 104 (1996) 5942.
[25] J.M. Papanikolas, P.E. Maslen and R. Parson, J. Chem. Phys. 102 (1995) 2452.
[26] A. Gallagher, Phys. Rev. 157 (1967) 68.
[27] E.A. Yukov, Sov. J. Quant. Electr. 3 (1973) 117.
[28] W.P. Hess, PhD thesis, University of Colorado (1988).
[29] V.S. Batista and D.F. Coker, J. Chem. Phys., in press.